Available online at www.sciencedirect.com
SCIENCE DIRECT®
Spectrochimica Acta Part A 60 (2004) 1359–1365
SPECTROCHIMICA ACTA PART A
www.elsevier.com/locate/saa

ESR studies of Anatolian gypsum

Ülkü Ulusoy*

Department of Physics Engineering, Hacettepe University, 06532 Beytepe, Ankara, Turkey

Received 15 July 2003; accepted 17 October 2003

Abstract

Electron spin resonance (ESR) was used to date the formation and most recent recrystallization of three types of gypsum samples (massive, bedded and fracture filling gypsum) from the Sakarya Formation at Eskişehir in the middle of Turkey. The ESR spectra had the signals of Fe^{3+} and Mn^{2+} in addition to those of the G1 and G2 sensitive centers ($g = 2.002$ and 2.008) to artificial γ-irradiation. ESR intensities of G1 and G2 were enhanced by γ-ray irradiation to give equivalent doses D_E for each sample. The ESR ages derived from the annual doses of ^{238}U, ^{232}Th and ^{40}K contents of the samples determined by thermal neutron activation analysis (TNAA) were between 43 ± 18 ka (massive gypsum) and 1100 ± 466 ka (bedded gypsum) as minimal and maximal values. The ages fall into the upper Miocene–Pliocene Epoch of the geological time scale, which agreed with the stratigraphy.

Keywords: Electron spin resonance (ESR); Dating; Gypsum; Annealing

1. Introduction

Gypsum, the dihydrate form of calcium sulfate ($CaSO_4 \cdot 2H_2O$, monoclinic) is a common sulfate mineral, which has different morphology including prismatic, rosette and other habits, and often forms through precipitation from saline waters in arid areas. Although different crystallization characteristics of gypsum may provide clues to the depositional environment during growth of the mineral, the conclusions about the depositional environments on gypsum habits is uncertain unless the chemical and physical factors producing these habits are understood [1]. The chronology of the gypsum deposits in quaternary arid areas is one of the significant factors for the study of environmental history.

Gypsum is useful for electron spin resonance (ESR) dating that has been widely applied to a number of different geological minerals for determining the chronology. Some of these applications for the stratighraphic gypsum have already been reported by Nambi [2], Ikeda et al. [3], Yijian et al. [4], Ikeda and Ikeya [5], Omura and Ikeya [6]. In this method, the concentration of accumulated defects having unpaired electrons produced by natural radiation after the crystallization is measured. The accumulated dose of natural radiation, D_E is obtained by the use of the additive dose method. Hence, the measurement sample acts as a dosimeter to record the dose from all radioactive elements such as U, Th and K in its immediate environment in radius up to 30 cm. The determination of the radioactive composition enable to calculate the contribution of the inherent dose to the annual dose, D, which includes the cosmic dose rate. The age T is then calculated from the equation: $T = D_E/D$ [7].

ESR provided some signals related to the accumulation of unpaired electrons at $g = 2.009$ (G2), 2.004 (G1) and 2.003 (G3), which were attributed the oxygen centers (O_3^{2}, O_2^{-} and O_3^{-} electron deficient centers) were reported for natural gypsum powders [8] and common anhydrite crystals ($CaSO_4$) by Bershov et al. [9], and Ikeda and Ikeya [5]. The applicability of ESR dating is directly related to the stability of these centers or its lifetime. For instance, the mean lifetime of the G1 at $g = 2.004$ approximately to 10^{12} years, whilst the G2 at $g = 2.009$ was reported to be more stable than the former [10]. By considering the concepts mentioned above, it is obvious that the gypsum minerals are suitable material for ESR dating studies.

Sivrihisar Neogen lacustrine basin of Sakarya Formation is one of the most typical Neogen basin in central Anatolia in Turkey. The basis contains evaporated formation such as

* Tel.: +90-312-297-6179; fax: +90-312-299-2037.
E-mail address: ulusoy@hacettepe.edu.tr (Ü. Ulusoy).

1386-1425/$ – see front matter © 2003 Elsevier B.V. All rights reserved.
doi:10.1016/j.saa.2003.10.034

dolomite, sepiolite and gypsum. The ESR signals of sepiolite from the basin and its dating were previously reported in detail [11]. The occurrences of gypsum should also provide unique examples of ancient lacustrine environment of the basin. In this study, the paramagnetic features of some typical gypsum from the Sakarya Formation were investigated in view of the ESR dating to be able to compare with the features of the sepiolite.

2. Experimental

2.1. Gypsum samples ($CaSO_4{\cdot}2H_2O$)

Some properties of the samples from Sazılar Village of Polatlı, Ankara and Sivrihisar–Eskişehir in Sakarya Formation are presented in Table 1. The formation consists of gypsum associated with dolomite, dolomite-bearing sepiolite and limestone in the Sivrihisar Lacustrine basin. Gypsum rocks present different crystallization characteristics. The morphology is characterized by marked variability and includes discoidal, prismatic, pyramidal, rosette and numerous other habits. Most gypsum is white to grayish white although the impurities in any given deposit frequently determine the color of the rock and resulting products. Sedimentological features of gypsum indicate different depositional environments such as sub-water, lacustrine plains and fracture-fillings. Three types of gypsum were defined in the formation [12]: the massive, the bedded, and the displacive-grown and fracture filling gypsums. The samples used in this investigation and its features in accordance with the gypsum types are given in Table 1.

2.2. Experimental procedure

The pieces of gypsum were picked up from the host rock (dolomite, dolomite-bearing sepiolite and limestone) and gently powdered. About 300 mg of 12–14 aliquots of each sample were used for γ-irradiation and annealing experiments. ESR measurements were performed with a Varian E-L9″ X-band ESR spectrometer at ambient temperature with a 100 kHz field modulation of amplitude at 0.8 mT and with a microwave power of 2 mW. The scan speed was 5 mT min^{-1} with a time constant of 1 s.

The samples were irradiated with different γ-doses of 0–3.2 kGy by the use of a ^{60}Co source with a rate of 2.15 kGy h^{-1}. Single growth curve was fitted to a saturation curve which was obtained by the least-square method by using a software. Values of D_E were determined by extrapolating the growth curve to the zero ordinate. Thermal stabilities of paramagnetic centers were scanned with the ESR measurements by isochronal annealing from 50 to 600 °C for 15 min at each step, and by isothermal annealing at the temperatures of 525, 550, 580 and 600 °C for different periods at each step.

Annual doses were calculated from ^{238}U, ^{232}Th and ^{40}K contents of the samples measured by thermal neutron

Table 1
Some properties of three types of gypsum which occur in many parts of the world, and has long been of economic importance in the family of industrial minerals

Sample code	Site	Color, morphology (crystal size) and host rock	Types of gypsum
T4	Sivrihisar–Eskişehir	Honey, prismatic (50 mm × 12 mm × 25 mm), too many very fine layers in the 25 mm thickness), dolomite	Bedded gypsum at the upper levels of massive gypsum(the thickness of 6 m)
T21	Sivrihisar–Eskişehir	White, prismatic (70 mm × 30 mm × 20 mm), dolomite	Bedded gypsum at the upper levels of massive gypsum(the thickness of 6 m)
T7-G	Sivrihisar–Eskişehir	Green, pyramidal (swallow tail, 95 mm × 50 mm × 20 mm), dolomite and limestone	Displacive-grown, fracture filling gypsum (the thickness of 20 m)
T7-B	Sivrihisar–Eskişehir	Brown or honey, pyramidal (swallow tail, 95 mm × 50 mm × 20 mm), dolomite and limestone	Displacive-grown, fracture filling gypsum (the thickness of 20 m)
T15	Sivrihisar–Eskişehir	Honey, rosette (55 mm × 45 mm × 30 mm) sdolomite	Displacive-grown, fracture filling gypsum (the thickness of 20 m)
T16	Sivrihisar–Eskişehir	White, discoidal (40 mm × 10 mm × 15 mm), dolomite	Displacive-grown, fracture filling gypsum (the thickness of 20 m)
T11	Sivrihisar–Eskişehir	White, pyramidal (swallow tail, 50 mm × 5–12 mm × 10 mm), dolomite and limestone	Displacive-grown, fracture filling gypsum (the thickness of 20 m)
T20	Sivrihisar–Eskişehir	White, prismatic (length< 0.5 mm, very fine crystals), dolomite	Massive gypsum (the thickness of 10 m)
1	Sazılar–Polatlı Ankara	White, prismatic (4 mm × 1.5 mm × 1 mm), dolomite	Massive gypsum (the thickness of 10 m)

It is generally calcined for the production of stucco for industrial applications. Uncalcined uses of gypsum are principally as a retarder for portland cement, as a soil conditioner, as a mineral filler, and other minor.

Table 2
Concentrations of radioactive elements obtained by thermal neutron activation analysis, calculated total annual doses including the cosmic dose rate (0.35 mGy a^{-1}), D_E's and ESR ages of the G1 and G2 centers in the gypsum samples

Sample code	^{238}U (ppm)	^{232}Th (ppm)	K (%)	Annual doses (mGy a^{-1})	D_E (kGy)		Age (ka)	
					G1	G2	G1	G2
T4	1.16 ± 0.21	–	0.07 ± 0.05	0.59 ± 0.05 (0.42 ± 0.02)	0.65 ± 0.22	0.08 ± 0.03	1100 ± 466 (1533 ± 587)	135 ± 62 (189 ± 79)
T21	1.25 ± 0.19	–	0.02 ± 0.05	0.60 ± 0.05 (0.42 ± 0.02)	0.25 ± 0.06	0.00 ± 0.01	417 ± 135 (595 ± 173)	1.00 ± 0.92 (1.43 ± 1.26)
T7-G	2.91 ± 0.15	–	0.07 ± 0.05	0.94 ± 0.04 (0.52 ± 0.02)	0.54 ± 0.12	0.14 ± 0.05	576 ± 152 (1038 ± 263)	149 ± 60 (269 ± 104)
T7-B	2.91 ± 0.15	–	0.07 ± 0.05	0.94 ± 0.04 (0.52 ± 0.02)	0.52 ± 0.20	0.02 ± 0.01	554 ± 237 (1000 ± 416)	20 ± 16 (37 ± 28)
T15	2.62 ± 0.16	1.51 ± 0.16	0.19 ± 0.03	1.01 ± 0.05 (0.56 ± 0.02)	0.33 ± 0.10	0.04 ± 0.02	327 ± 115 (589 ± 200)	40 ± 22 (71 ± 38)
T16	6.36 ± 0.14	1.41 ± 0.06	0.17 ± 0.03	1.74 ± 0.04 (0.76 ± 0.02)	0.42 ± 0.06	0.02 ± 0.02	242 ± 39 (553± 90)	12 ± 12 (26 ± 25)
T11	–	–	0.11 ± 0.04	0.37 ± 0.01 (0.76 ± 0.02)	0.06 ± 0.03	0.03 ± 0.03	162 ± 86 (553± 90)	78 ± 78 (26 ± 25)
T20	6.41 ± 0.18	–	0.02 ± 0.05	1.97 ± 0.08 (0.78 ± 0.05)	0.20 ± 0.06	0.01 ± 0.01	102 ± 34 (258 ± 94)	6 ± 7 (15 ± 18)
1	2.48 ± 0.16	0.94 ± 0.09	0.19 ± 0.03	1.13 ± 0.07 (0.65 ± 0.03)	0.05 ± 0.02	0.12 ± 0.06	43 ± 18 (75 ± 31)	105 ± 56 (183 ± 97)

Annual doses were calculated assuming both ways of 100% loss of Rn in parentheses and no loss of Rn.

activation analysis (TNAA), using the conversion table given by Nambi and Aitken [13]. In this calculation, we used the conversion factors assuming both ways of no Rn loss and 100% Rn loss. The efficiency of the defect production by α-rays (*k* value) in gypsum is tentatively estimated to 0.05, as in calcite [14]. The attenuation factor for the average γ-doses was assumed to be 0.78 for the sample thickness of 15 mm or thicker ones, using Fig. 3a of Grün [15]. The attenuation factors for the β-rays for different sizes of the samples were considered to be the values of Table 2 in Mejdahl [16]. The calculated total annual doses for the buried samples are provided in Table 2. The contribution of the cosmic dose to the dose rates was considered to be 0.35 mGy a^{-1} by assuming the elevation, latitude and depth (1000 m, 39° and 17 g cm^{-2}) of the sampling site [17–19].

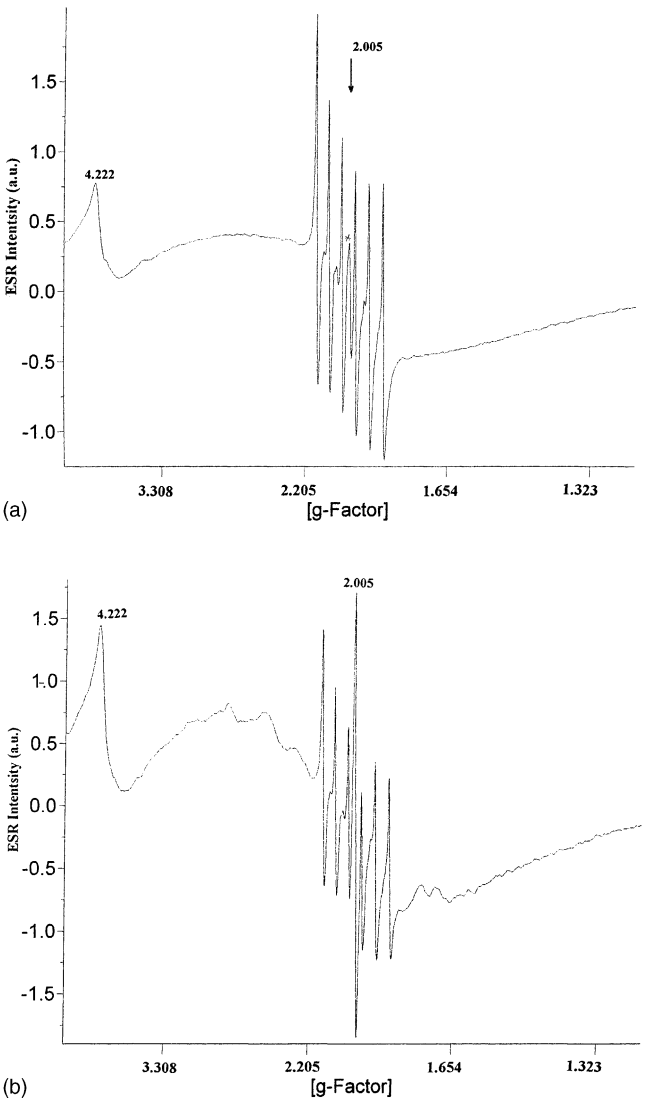

Fig. 1. ESR spectrum of the sextet of hyperfine lines attributed to Mn^{2+} in addition to the Fe^{3+} peak at $g = 4.22$ observed in powdered natural gypsum sample T15 at room temperature. (a) Natural sample, (b) 1.61 kGy γ-irradiated sample. The characteristic peaks for dating are observed at about $g = 2.005$ in the middle of the sextet of hyperfine lines.

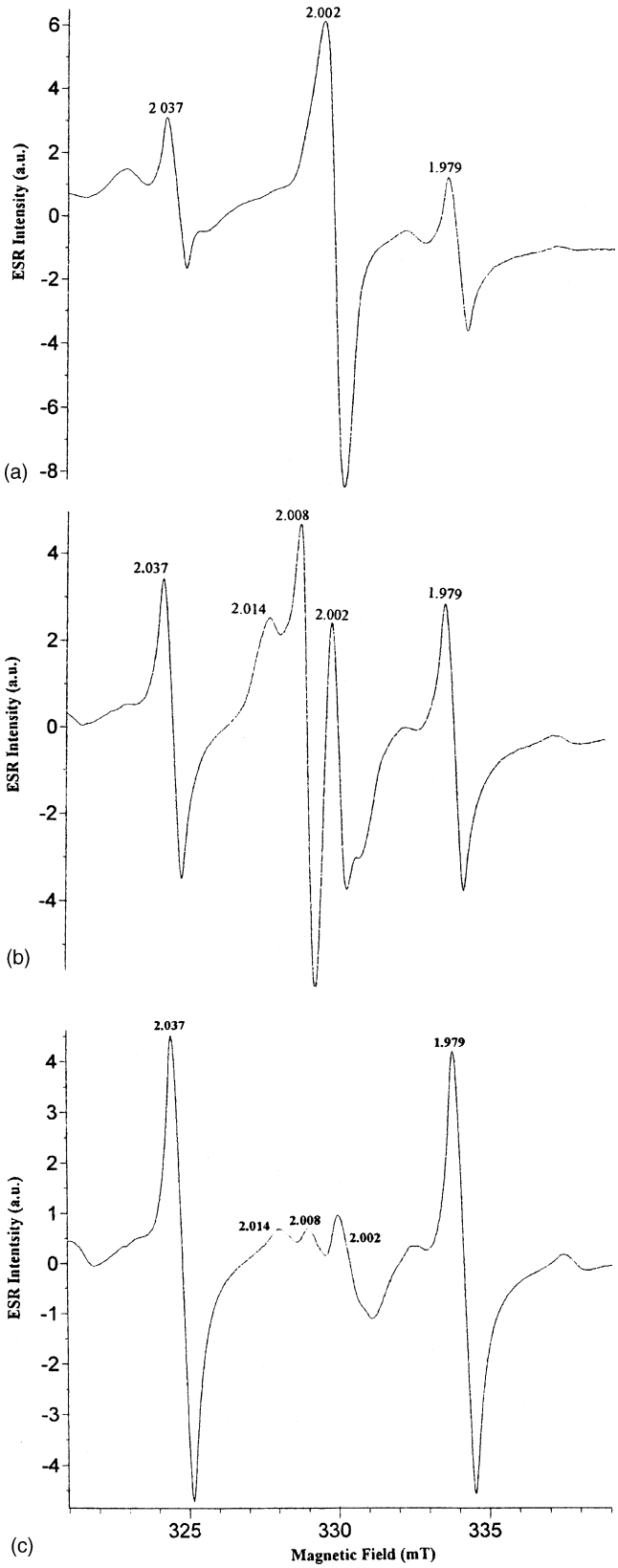

Fig. 2. ESR spectra of gypsum sample T15 for (a) natural, (b) γ-irradiated at 1.61 kGy and (c) 1.61 kGy γ-irradiated-heated at 600 °C for 9 min. The intensities of the signals at $g = 2.008$ and 2.002 of the natural sample increased by γ-rays, while the signal at 2.002 disappeared after annealing at 600 °C.

3. Results

3.1. ESR signals and equivalent dose (D_E)

The ESR spectra of T15 for natural and 1.61 kGy γ-irradiated powdered gypsum samples are shown in Fig. 1a and b. The characteristic peaks for the sample are observed at $g = 2.005$ in the middle of the sextet of hyperfine lines of Mn^{2+}, in addition to the peak at $g = 4.22$ presumably associated with Fe^{3+}.

The ESR spectra of the natural samples were compared with those of the samples exposed to 1.61 kGy and the exposed and annualed in for 600 °C for 9 min (Fig. 2a–c). Two centers were seen in Fig. 2a, the one at $g = 2.014$ to 2.008 for G2, and the other $g = 2.002$ for G1, which were between third and fourth of sextet hyperfine lines of Mn^{2+} ($g = 2.037$ and 1.979). These centers were sensitive, for which the increase at $g = 2.008$ and 2.002 of the irradiated sample (Fig. 2b), and the disappearence of the signal at $g = 2.008$ of the annealed sample (Fig. 2c) were evident. However, the intensities of Mn^{2+} and Fe^{3+} signal were remained unchanged in all samples.

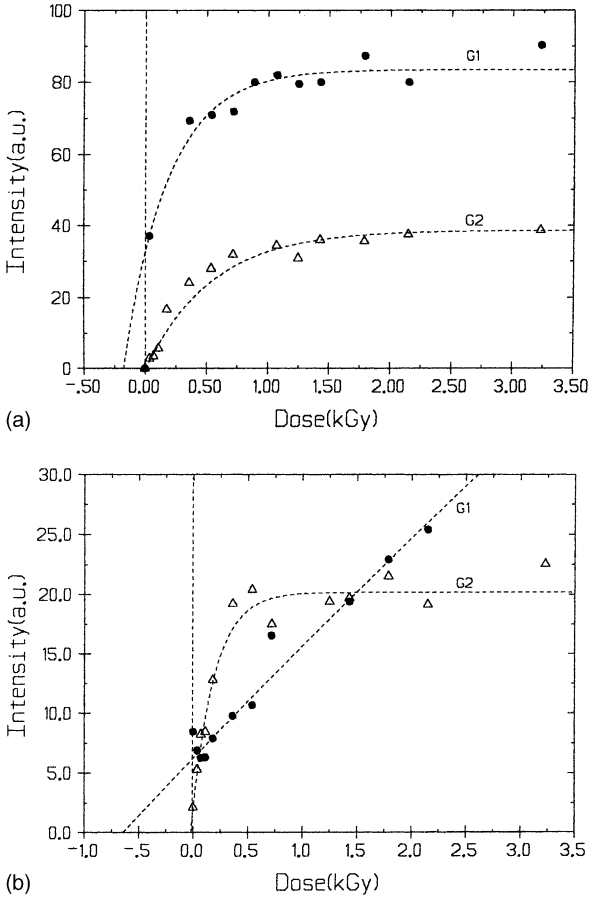

Fig. 3. Growth curves of the G1 and G2 centers in the gypsum samples. (a) T20 of massive gypsum. The intensity increased exponentially by γ-doses; (b) T7-B of fracture filling gypsum. The intensities of G2 in T7-B enhanced exponentially, while G1 increased linearly by γ-doses.

In all samples the ESR intensities of the sensitive centers increased exponentially (Fig. 3a for T20), whilst those for G1 in T4 and T7-B which increased linearly by γ-ray irradiation (Fig. 3b for T7-B). The signals of G2 in natural T16 and T21, and G1 and G2 in natural T20 could not be recorded.

Table 2 summaries the calculated values of D_E and ages in addition to the annual doses calculated by using radioactive contents for each sample. Since the values of D_E for the G2 of T20 and T21 were close to zero, the ages should be zero with the 100% error limits. The age distribution of the studied samples is shown in Fig. 4. The ages of the centers present different values from 1.0 ± 0.9 ka to 1100 ± 466 ka though they fall into the same Neocene basins. On the other way, the ages of G2 centers within the 1.0 ± 0.9 ka to 135 ± 62 ka limits are younger than those of G1 centers in the range of 43 ± 18 ka to 1100 ± 466 ka.

3.2. Thermal stabilities of the centers

The isochronal annealing experiments of G1 and G2 for the sample 1 from the massive gypsums are shown in Fig. 5. The signal intensities of G1 did not change up to 500 °C, after this temperature they significantly increased and continued by the increasing temperature to 600 °C. The increase were also observed for G2 centers. The increase was started above 450 °C, reached maximum at about 550 °C and disappeared completely at 600 °C.

Isothermal annealing experiments showed that the intensities of G1 increased at the first step, then decreased by heating periods at 525, 550, 580 and 600 °C, whilst they increased again after decreasing by heating periods at 600 °C (Fig. 6). However, G2 annealed at these temperatures. The decay coefficients of G1 centers were calculated by assuming the annealing obeys first-order kinetics and the results were plotted on an Arrhenius diagram (Fig. 7). The mean lifetime, τ at an average environmental temperature of

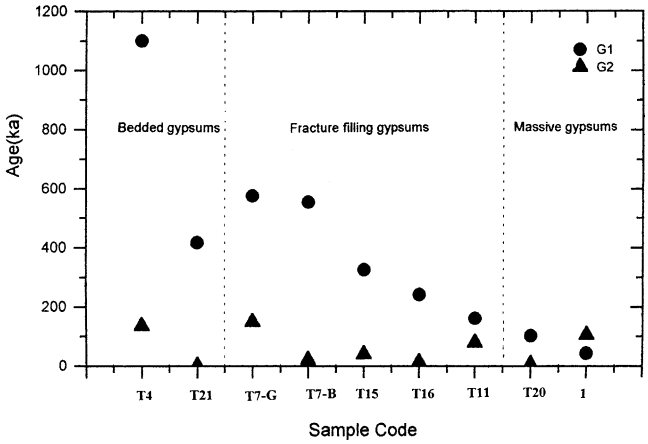

Fig. 4. The ages calculated for different types of gypsum samples are presented vs. the sample code. According to the data, the youngest and oldest gypsum belong to the massive and bedded gypsum, respectively.

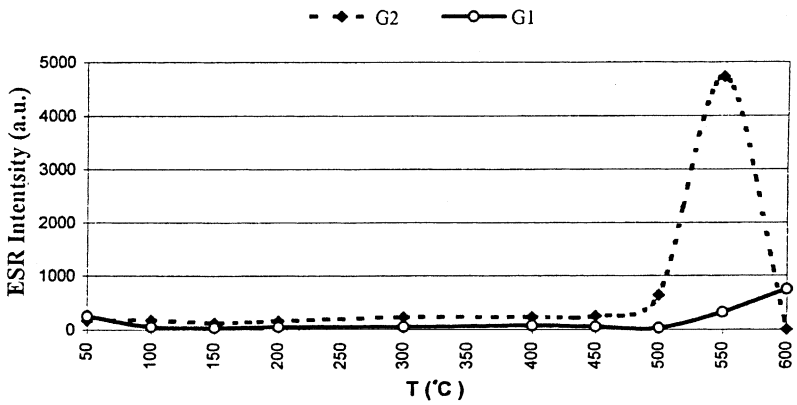

Fig. 5. Signal variations on isochronal annealing experiments for 15 min. The intensity of G2 reached its maximal value at 550 °C and then disappeared at 600 °C, while the intensity of the G1 continued to increase even at the temperatures of 600 °C.

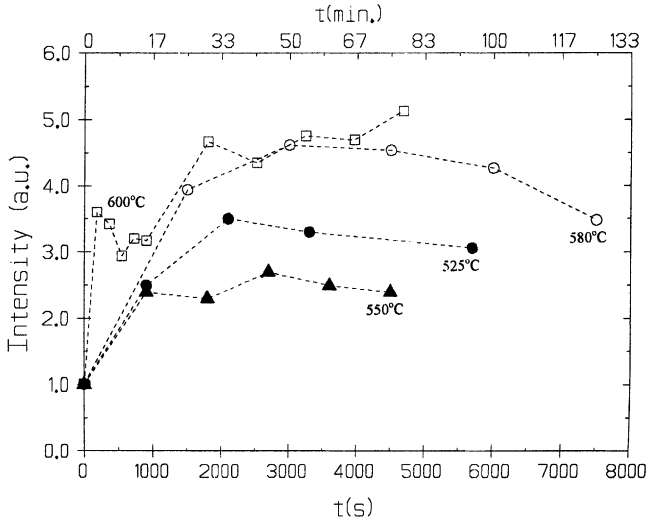

Fig. 6. The variations of the intensities of G1 in the sample 1 on the isothermal annealing experiments.

15 °C, activation energy, E and frequency factor, $1/\tau_o$ were found to be 2.4×10^{21} years, 2.2 eV and $2.1 \times 10^9\,s^{-1}$, respectively.

4. Discussions

Three types of gypsum samples from the Sakarya Formation falling into the upper Miocene–Pliocene of Neocene lacustrine basins were studied. The ESR results showed that the samples had two sensitive centers, G1 and G2 in addition to the ones of Mn^2 and Fe^{3+} which were stable. There were no relation between samples and its spectra.

The ESR ages calculated for the G1 and G2 varied in a wide range (Table 2 and Fig. 4). The ages of the G2 centers were within the range of 1.0 ± 0.9 ka to 135 ± 62 ka, and those of G1 were of 43 ± 18 ka to 1100 ± 466 ka.

The ages of the G2 centers in three types of the samples were younger than those of G1 with the mean lifetime of 2.4×10^{21} years. This should be due to the difference in thermal stability of the centers. However, Nambi [10] suggested that G2 signal at 2.008 is more stable than G3 at $g = 2.004$ with the mean lifetime of 10^{12} years and can be used for ESR dating. Therefore, the ages of G1 centers may be accepted as the reliable ages of the samples, whilst G2 centers might be considered to be annealed after the formation of the crystals. However, the signals of G2 was too weak but those of G1 were observed clearly in all the natural samples. The ages of G2 in the samples from massive gypsums (T20), bedded gypsums (T21) and fracture filling gypsums (T16) were calculated within 100% errors. The massive gypsums had the finest crystals amongst the studied types and had the youngest ages in view of both centers. This might imply that the massive gypsums was possibly recrystallized repeatedly under the environmental conditions of lake and ground water, after its formation in the upper Miocene–Pliocene Epoch, but was not annealed due to the subjection of high temperatures like a few hundred degree celsius, in this period. Based on this possibility, it can be concluded that sample T4 of the bedded gypsum and sample 1 of the massive gypsum were the oldest and youngest ESR age of G1; 1100 ± 466 ka and 43 ± 18 ka. The ages of the formation for bedded, fracture filling and massive gypsums might be within the range of 417 ± 135 ka to 1100 ± 466 ka, 162 ± 86 ka to 576 ± 152 ka, and 43 ± 18 ka to 102 ± 34 ka, respectively. Three types of gypsums can be classified chronologically as the bedded, the fracture filling and the massive gypsums from its formation to the present.

These ages of the site are young due to the recrystallization or annealing effects in the site though they are in agreement with the stratigraphy. On the other hand, the ages are in good agreement with the ages of three types of sepiolites for the same formation, 1800 ± 800 ka, 900 ± 200 ka and 700 ± 500 ka for beige sepiolites, meerschaum and brown sepiolites, respectively [11].

The major disadvantage of the ESR age determination is that the method requires further consideration past dose rates for an inhomogeneous site. The inhomogeneity of

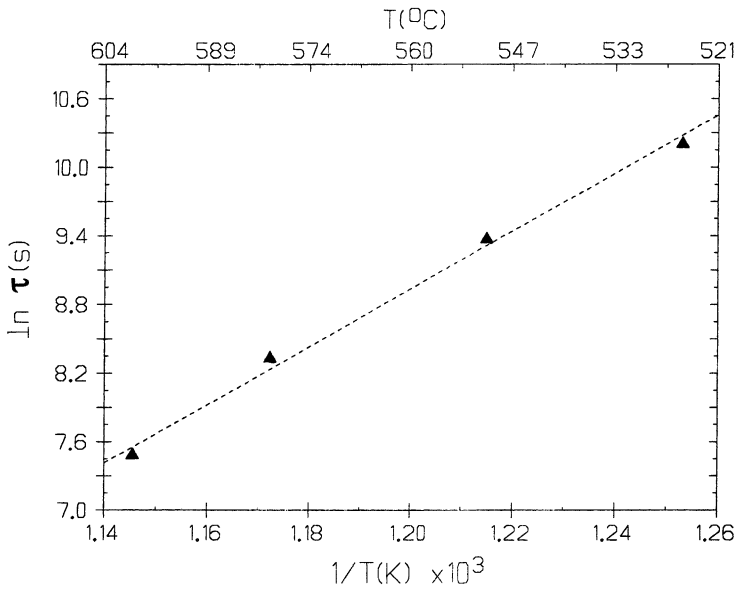

Fig. 7. Arrhenius diagram of decay coefficients of G1. First-order kinetics was assumed when calculating the coefficients for the decay curve. An activation energy of 2.2 eV and a frequency factor of $2.1 \times 109\,s^{-1}$ were obtained by fitting a line to those points by the least-square method. Extrapolating this line to 15 °C, the mean life time of the center was calculated to be 2.4×10^{21} years.

radioactive contents in host rocks and gypsum crystals may cause a wide scatter of ESR data. For confirmation of the ESR ages of the studied site, the age determination by different techniques, like ^{14}C is required.

Acknowledgements

I would like to express my gratitude to Professor Dr. Y. Erkan and his graduate student, T. Altay (Department of Geology at Hacettepe University, Ankara, Turkey) for supplying the gypsum, and to Professor Dr. M. Bichler (Atominstitute of Austrian University in Vienna, Austria) and H. Tatlısu (Vienna Technical University, Austria) for analyzing the samples by TNAA. I would also like to extend my thanks to Dr. U. Ulusoy (Department of Chemistry at Cumhuriyet University, Sivas, Turkey) for his help in improving the original manuscript considerably.

References

[1] R.D. Cody, A.M. Cody, J. Sediment. Petrol. 58 (2) (1988) 247–255.
[2] K.S.V. Nambi, PACT 6 (1982) 314–321.
[3] S. Ikeda, M. Ikeya, N. Kashima, J. Speleol. Soc. Jpn. 14 (1989) 68.
[4] C. Yijian, A.V. Arakel, Lu Jinfen, Appl. Radiat. Isot. 40 (10/12) (1989) 1163–1170.
[5] S. Ikeda, M. Ikeya, Jpn. J. Appl. Phys. 31 (1992) L136–L138.
[6] T. Omura, M. Ikeya, Geochem. J. 29 (1995) 317–324.
[7] M. Ikeya, New Applications of Electron Spin Resonance. Dating, Dosimetry and Microscopy, World Scientific, Singapore, 1993.
[8] M. Kasuya, S. Brumby, J. Chappel, Nucl. Tracks Rad. Meas. 18 (1991) 329.
[9] L.V. Bershov, V.O. Martirosyan, A.S. Marfunin, A.V. Speranskii, Fortschr. Miner. 52 (1975) 591–604.
[10] K.S.V. Nambi, Nucl. Tracks 10 (1985) 113–131.
[11] Ü. Ulusoy, M. Ikeya, Appl. Magn. Reson. 18 (2000) 537–548.
[12] Z. Karakaş, Yerbilimleri (Geosound) June No: 30 (1997) 743-754 (in Turkish with English abstract).
[13] K.S.V. Nambi, M.J. Aitken, Archaeometry 28 (2) (1986) 202–205.
[14] R.G. Lyons, B.J. Brennan, Nucl. Tracks Radiat. Meas. 18 (1991) 223–227.
[15] R. Grün, Quaternary Int. 1 (1989) 65–109.
[16] V. Mejdahl, Archaeometry 21 (1) (1979) 61–72.
[17] J.R. Prescott, L.G. Stephan, PACT 6 (1982) 17–25.
[18] J.R. Prescott, J.T. Hutton, Nucl. Tracks Radiat. Meas. 14–1/2 (1988) 223–227.
[19] J.R. Prescott, J.T. Hutton, Radiat. Meas. 23–2/3 (1994) 497–500.